ANALYSIS OF A DEORBITING MANEUVER OF A LARGE TARGET SATELLITE USING A CHASER SATELLITE WITH A ROBOT ARM

Philipp Gahbler[1], **R. Lampariello**[1], **and J. Sommer**[2]

[1]*German Aerospace Agency (DLR), Institute for Robotis and Mechatronics, Germany*
[2]*ASTRIUM Space Transportation GmbH, Bremen, Germany*

ABSTRACT

The purpose of this analysis is to examine whether Chaser satellite equipped with a robot arm can be used to perform a deorbiting maneuver on a very heavy Target satellite. For this, two aspects are analyzed: the system response at the beginning and end of a thrust profile and the effects of an external torque caused by a misalignment of the two bodies.
The dynamics of the system are examined analytically and subsequently verified in a numerical multi-body simulation.
The results show that the system is inherently stable and needs very little intervention by the robot. With a particular off-modulation of the thrusters, separation between the two satellites can be avoided, without intervention of the robot.

1. INTRODUCTION

The deorbiting of defective satellites may play a vital role in the fight against space debris. A promising approach for this task is the use of a chaser satellite equipped with a robot arm. Since such a maneuver has never been attempted, it is important to examine whether such a task can be performed safely. To our knowledge, this hasn't been examined previously.
The model that was assumed consists of a heavy target satellite and a chaser, which establishes a connection to the target through surface contact and a robot arm. The chaser uses four orbit control thrusters to propel the entire system and transfer it into a lower orbit. The thrust force is transferred through the surface contact. The purpose of the robot next to performing the capture of the target is only that of stabilizing the system.
The principal question examined is, whether the system remains stable. For this, the two satellites must remain in contact at all times and cannot spin out of control. This must be done using a relatively weak robot, which can only exert a fraction of the forces used to propel the system.
Two critical aspects have been identified: the release of potential energy at the end of a thrust profile and the influence of external torque caused by a misalignment of the thrust vector in relation to the system center of mass.

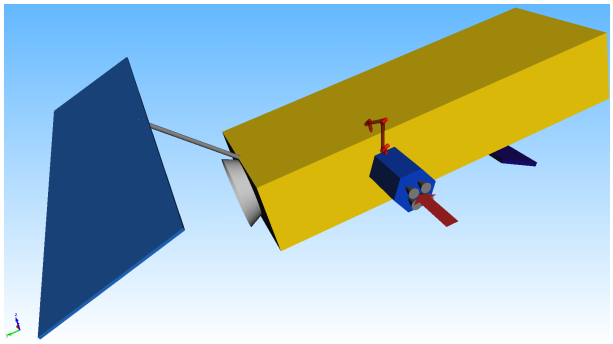

Figure 1: Model of the system with large target satellite and chaser satellite (with 7 dof robot arm) resting in proximity of the former's centre of mass shown. Red arrow shows direction of deorbiting thrust force.

Section 2 addresses the one-dimensional dynamics of a mass-spring-damper system that results from the natural elasticity in the surface contact. Section 3 examines the three-dimensional dynamics of external torques caused by a misalignment of the thrust vector in relation to the system center of mass as well as the internal forces and torques caused by these effects. Section 4 shows the thrust profile which results from a typical off-modulation controller to account for the misalignment. Section 5 validates the analytical results of the previous Sections with help of the numeric multi-body simulation program *Simpack*. Section 6 draws the conclusions and refers to future work.

2. THE ONE-DIMENSIONAL DYNAMICS

In this section the one-dimensional dynamics that result from a mass-spring-damper system consisting of the two satellites in contact with each other during the deorbiting maneuver is analyzed. The stiffness resulting from the structural elasticity of the satellites is assumed to be very high.
First the mathematical properties of the system are established in 2.1, after which the critical phases, when the thrust commences 2.2.1 and when it ceases 2.2.2, are ex-

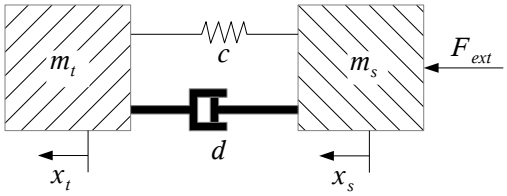

Figure 2: Spring-damper system

amined and it is shown that these dynamics can be controlled with the help of the robot. In 2.2.3 the system response to a modulated thrust profile is examined.

2.1. Equations of Motion

The (internal) contact force f_c is modelled using linear spring-damper coefficients:

$$f_c = c\Delta x + d\Delta\dot{x} \tag{1}$$

where $\Delta x = x_t - x_s$ is the relative distance between the bodies and c, d are the spring and damper constants resulting from the structural elasticity and damping. Since the force only acts during compression it has the condition $\Delta x \leq 0$.
The equation of motion for the target is:

$$m_t\ddot{x}_t = f_c \tag{2}$$

and for the Chaser:

$$m_s\ddot{x}_s = -f_c + F_{thr} \tag{3}$$

m_t and x_t are the mass and absolute position of the target, m_s and x_s of the Chaser. F_{thr} is the (external) thrust force used to propel the system. The relative acceleration $\Delta\ddot{x}$ is gained by subtracting (2) - (3) :

$$\Delta\ddot{x} = (\frac{m_t + m_s}{m_t m_s})f_c - \frac{1}{m_s}F_{thr} \tag{4}$$

With the expression $\tilde{m} = \frac{m_t m_s}{m_t + m_s}$ the following differential equation results:

$$\tilde{m}\Delta\ddot{x} + d\Delta\dot{x} + c\Delta x = -\frac{\tilde{m}}{m_s}F_{thr}(t) \tag{5}$$

Using $\omega_0 = \sqrt{\frac{c}{\tilde{m}}}$ and $\delta = \frac{d}{2\sqrt{\tilde{m}c}}$ the equation is:

$$\Delta\ddot{x} + 2\omega_0\delta\Delta\dot{x} + \omega_0^2\Delta x = -\frac{1}{m_s}F_{ext}(t) \tag{6}$$

If the system is underdamped ($\delta < 1$) the following step response $h(t)$ occurs:

$$h(t) = A \cdot [1 - (1-\delta^2)^{-\frac{1}{2}}\, e^{-\delta\omega_o} sin(\omega_d t + \psi)] \tag{7}$$

with $\psi = \arccos(\delta)$, $\omega_d = \omega_0\sqrt{1-\delta^2}$; the amplitude A is:

$$A = -\frac{1}{\omega_0^2} \cdot \frac{1}{m_s}F_{ext} = -\frac{1}{c} \cdot \frac{m_t}{m_t + m_s}F_{ext} \tag{8}$$

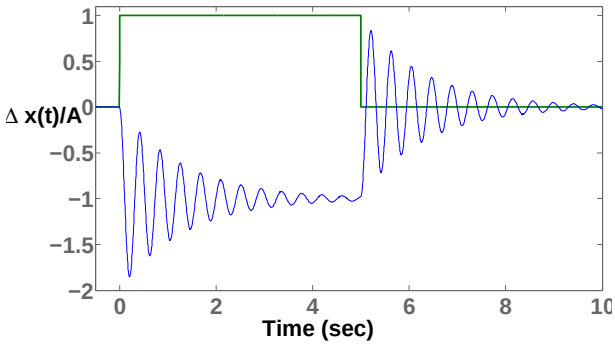

Figure 3: 1D spring-damper system response to a rectangle input

2.2. Conditions at the Beginning and End of a Thrust Profile

It is important to examine the value of Δx in relation to the thrust in order to identify occasions where the two bodies might separate. The significant situations are the beginning and the end of the thrust profile. Figure 3 shows the system response (with an arbitrary frequency) at these points.

2.2.1. Beginning of Thrust Profile

With the initial conditions $\Delta x_0 = 0$ and $\Delta\dot{x}_0 = 0$ the step response oscillates about the steady state $\Delta x_f = A$ with an amplitude of A. Therefore Δx is always within the range $0 \geq \Delta x > 2A$. This means that while a constant thrust is applied the relative distance is always negative and the system in contact.

2.2.2. End of Thrust Profile

When the thrust stops, the potential energy stored in the structure is released. This would cause the masses to drift apart. However, if high stiffness is assumed, the stored energy is low. The following formula calculates the potential energy of the system (having reached the steady state):

$$E = \frac{1}{2c}F_{thr}^2 \tag{9}$$

If a stiffness of $1.0 \times 10^8 \frac{\mathrm{N}}{\mathrm{m}}$ and a thrust of 1500 N are assumed, the stored energy has a value of 11.25 mJ. A robot exerting a maximum force of 10 N could compensate this amount of energy over a distance of 2.3 mm! This shows, that despite the high forces involved, the high stiffness reduces the stored potential energy. A robot using a small force can decelerate the masses and bring them back together over a short distance.

2.2.3. Modulated Thrust Profile

The modulation described in Section 4 selectively turns off one or several of the Chaser's four thrusters. The reduction in thrust releases potential energy, similar to the

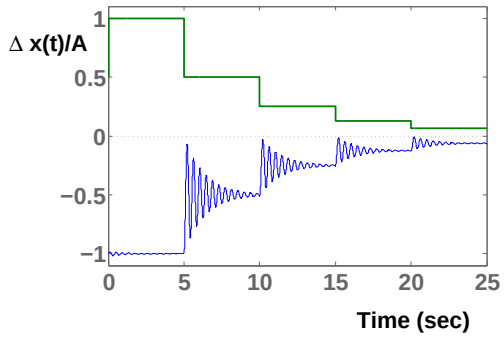

Figure 4: 1D spring-damper system response to a reduction of the thrust by half of the current value

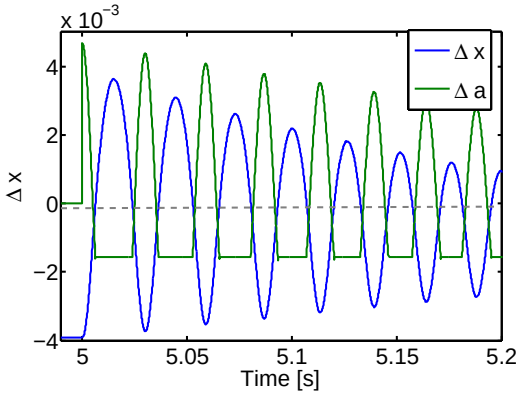

Figure 5: The oscillation that follows a reduction of the thrust. At the time of 5 s the thrust was reduced to a level of 0.25 of the former. Δx consists of parabolic and sinusoidal sections.

case described in 2.2.2. However, the thrust never goes to zero since at least one thruster is on at all times.
When the thrust is reduced by a step, the spring-damper system oscillates about the difference of the previous steady state to the current. Therefore, if the thrust is reduced by less than half of the overall thrust, the relative distance is negative and the system remains in contact at all times. This can be seen in Figure 4.
Therefore, there are only two steps that need to be avoided during the modulation: A reduction from four thrusters to one thruster and a reduction of three thrusters to one thruster. All other steps are safe.
A condition for the safety of the steps is that the system has reached its steady state before the next step is performed. This is very likely for the thruster modulation, since the high stiffness of the structure causes a high frequency of oscillation. The thruster modulation can be performed at a fairly low frequency (an example of 1 Hz is used in Section 4). This gives the system ample time to reach the steady state.
This means that a modulation of the thrusters can be configured to avoid the danger of separation at all times.

Figure 5 shows the oscillation that follows a reduction of the thrust by more than half. This leads to a separation of the two bodies. During this phase no force acts on the Target mass. The Chaser, however, is still accelerated by the (reduced) thrust. Therefore the relative acceleration is constant and negative. The relative distance between the two masses thus has a parabolic section. Once Δx crosses back into the negative and the bodies re-establish contact. This leads to a harmonic section with a sinusoidal profile for acceleration and position. The oscillation consisting of parabolic and sinusoidal sections is dampened only when the masses are in contact, so its amplitude is gradually reduced.

3. THE THREE-DIMENSIONAL DYNAMICS

This Section covers the three-dimensional dynamics of the combined system. The causes for external torques and their effects are analyzed. The internal forces resulting from these torques are examined in two cases: with presence of friction and without friction.
The chaser that is used for the analysis has four Orbit-Control Thrusters, which its attitude controller can selectively turn off in order to create control torques (Off-Modulation). The causes of external torques are investigated in 3.1. The effects of external torque are analyzed in 3.2. Finally, the Subsection 3.3 looks specifically at the lateral forces arising from the system's accelerations and how they are compensated, both in the case with friction (3.3.1) and without friction (3.3.2)

3.1. Causes of External Torques and their Effects

External torques occur when the chaser provides a thrust force that isn't directed through the center of mass (CoM) of the combined system. While the two satellites need to be aligned so that external torque is reduced, a degree of uncertainty remains since the CoM of the Target isn't necessarily known within a sufficient degree of accuracy. The torque caused by a deviation of the system CoM in relation to the thrust vector is:

$$\tau_{ext} = \mathbf{r}_{dev} \times \mathbf{F}_{thr} \tag{10}$$

The thrust vector only points in the x-direction, so that $\mathbf{F}_{thr} = [F_{thr}\ 0\ 0]^T$; $\mathbf{r}_{dev}$ is the vector of the deviation. Because of this the torque will only act about the y- or z-axis and the x-component of $\mathbf{r}_{dev}$ isn't relevant.
The external torque causes an angular acceleration of the system and subsequently an angular velocity about the system CoM following Euler's equation for the change in angular momentum:

$$\mathbf{I}_{sys}\dot{\omega}_s + \omega_s \times \mathbf{I}_{sys}\omega_s = \tau_{ext} \tag{11}$$

$\mathbf{I}_{sys}$ is the inertia tensor of the system, $\dot{\omega}_s$ and ω_s the system angular acceleration and angular velocity. If $\mathbf{I}_{sys}$ is nearly diagonal and ω_s is initially zero and $\tau_{ext,x} = 0$, the following assumption can be made for brief periods of time:

$$\dot{\omega}_s \approx \mathbf{I}_{sys}^{-1}\tau_{ext} \tag{12}$$

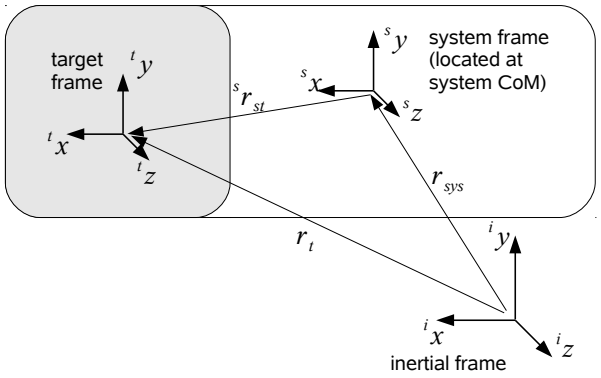

Figure 6: Relationship between the coordinate frames

This can be used to approximate the lateral forces the system experiences initially and is referenced in eq. (17)
The acceleration $\ddot{\mathbf{r}}_t$ that the Target experiences due to angular acceleration and velocity as well as the linear acceleration caused by the thrusters is:

$$\ddot{\mathbf{r}}_t = \ddot{\mathbf{r}}_{sys} + \dot{\omega}_s \times \mathbf{r}_{st} + \omega_s \times (\omega_s \times \mathbf{r}_{st}) \tag{13}$$

where $\ddot{\mathbf{r}}_{sys}$ is the linear acceleration of the system and $\mathbf{r}_{st}$ is the radius from the system CoM to the Target's CoM; $\dot{\mathbf{r}}_{st} = 0$ is assumed. Since no external forces act directly on the Target the sum of all internal forces transmitted between the chaser and the Target is:

$$\sum \mathbf{F}_t = m_t \ddot{\mathbf{r}}_t \tag{14}$$

The sum of torques on the Target mass is equivalent to eq. (11):

$$\sum \tau_t = \mathbf{I}_t \dot{\omega}_s + \omega_s \times \mathbf{I}_t \omega_s \tag{15}$$

since the angular acceleration and velocity is the same for all bodies in the system; $\mathbf{I}_t$ is the inertia tensor of the Target. With the assumption that the x-component of $\dot{\omega}$ and ω is roughly zero and that the vector $\mathbf{r}_{st}$ points mainly in the x-direction a few predictions about the directions of the inertial forces (given in the body frame of the system) resulting from the accelerations in eq. (13) can be made:

- $m_t \ddot{\mathbf{r}}_s$ points in the x-direction *(due to thrust force)*
- $m_t \dot{\omega}_s \times \mathbf{r}_{st}$ points in the y- or z-direction
- $m_t \omega_s \times (\omega_s \times \mathbf{r}_{st})$ points in the x-direction and opposes the thrust force

3.2. Balance of Internal Forces and Torques between the two Bodies

Assuming that the Target mass is static within the system, the inertial forces and torques discussed in Subsection 3.1 must be balanced by internal forces and torques. In order to calculate these, the two bodies are separated in the contact and the internal forces and torques are treated as external ones. This creates six equations that must be balanced.
The forces in the x-direction are normal forces which are transmitted by the surface contacts. The forces in the y- and z-direction are lateral forces and are transmitted by friction and/or the robot. Subsection 3.3 will discuss the distinction between forces provided by the robot and by friction.
Torques in the y- or z-directions are balances by the surface contacts, provided there are at least thee contact points arranged over an area. A torque about the x-axis would be compensated by friction. In the frictionless case the robot must provide a robot torque to create a balance about this axis.
The sum of all forces $\sum \mathbf{F}_t$ (eq. (14)) and all torques $\sum \tau_t$ (eq. (15)) acting on the Target give six constraints that must be met by the internal forces and toques acting between the two bodies:

$$\underbrace{\begin{bmatrix} 1 & 1 & \dots & 1 & 0 & 0 & 0 \\ 0 & 0 & \dots & 0 & 1 & 0 & 0 \\ 0 & 0 & \dots & 0 & 0 & 1 & 0 \\ 0 & 0 & \dots & 0 & -r_{l,z} & r_{l,y} & 1 \\ r_{1,z} & r_{2,z} & \dots & r_{n,z} & 0 & -r_{l,x} & 0 \\ -r_{1,y} & -r_{2,y} & \dots & -r_{n,y} & r_{l,x} & 0 & 0 \end{bmatrix}}_{6\times(n+3)} \cdot \underbrace{\begin{bmatrix} F_{c,1} \\ F_{c,2} \\ \vdots \\ F_{c,n} \\ F_{l,y} \\ F_{l,z} \\ \tau_x \end{bmatrix}}_{(n+3)\times 1} = \underbrace{\begin{bmatrix} \sum \mathbf{F}_t \\ \\ \sum \tau_t \end{bmatrix}}_{6\times 1} \tag{16}$$

$F_{c,1} \dots F_{c,n}$ are the n contact forces, $\mathbf{r}_1 \dots \mathbf{r}_n$ are the vectors from each contact point to the Target CoM. $F_{l,y}$ and $F_{l,z}$ are the lateral forces in y- and z-direction, $r_{l,y}$ and $r_{l,z}$ their vectors. τ_x is an internal torque, provided by either friction or the robot, needed to balance the system.
If number of contact forces n is smaller than three no solution exists. An n of three provides an exact solution while the addition of further contact forces creates redundancy in the system that can be solved numerically. This shows that the forces in x-direction are compensated by the contact forces. The lateral forces in the y- and z-direction only depend on the net force in that direction while the contact forces provide a balance of the torques in y- and z-direction. The balance of torques in the x-direction needs an additional term τ_x. The source of this torque and the lateral forces is discussed in the next subsection.

3.3. Lateral Forces

Equation (16) shows that there is a need for lateral forces in the y- and z-direction to compensate inertial forces, as well as a torque τ_x which balances the sum of torques in that direction. The forces and the torque can either be provided by friction or by the robot.
Based on the predictions made in Subsection 3.1 the term $\dot{\omega}_s \times \mathbf{r}_{st}$ is mainly responsible for lateral forces. Using equations (10) and (12) this can be formulated as:

$$\mathbf{F}_l \approx m_t \cdot \mathbf{I}_{sys}^{-1} (\mathbf{r}_{dev} \times \mathbf{F}_{thr}) \times \mathbf{r}_{st} \tag{17}$$

Since $\mathbf{r}_{st}$ and $\mathbf{I}_{sys}$ are constants, the lateral forces mainly depend on the thrust force $\mathbf{F}_{thr}$ and the deviation $\mathbf{r}_{dev}$. The numeric examples in Section 5.2.1 show that the following approximation for the magnitude of the lateral forces in relation to the normal forces can be made:
$F_l < 0.1 \cdot F_N$.
The necessary torque τ_x depends on the lateral forces and their point of application.

3.3.1. Friction

The maximum force of friction $\mathbf{F}_{fr,max}$ between two bodies is dependent on the normal force $\mathbf{F}_N$ in the contact surface and the coefficient of friction μ:

$$\mathbf{F}_{fr,max} = \mu \cdot \mathbf{F}_N \tag{18}$$

If a typical μ of 0.5 is assumed, friction can easily handle the lateral forces. The magnitude of the lateral forces is dependent on the thrust force as is the normal force. Friction can also provide the necessary torque in the x-direction needed to balance the system. It is assumed that the forces of friction act at each of the contact points. Since friction is a reaction force, the individual forces at each point will assume a value that balances the sum of forces in the y- and z-direction and the sum of torques about the x-axis.
If strong friction is present, there is no need for the robot to provide forces to balance the system.

3.3.2. Frictionless Case

If a smooth surface without friction is assumed the robot would have to handle the lateral forces and the torque about the x-axis. The forces required to compensate all lateral forces as calculated with eq. (16) would be somewhat high, as Section 5 shows.
With a robot grasping point that has a component in the y- and z-direction, a lateral force applied by the robot in one of those directions also creates a torque about the x-axis. Therefore the robot needs to provide a torque τ_x to ensure the balance of this component. This is the term featured in equation (16).
However, in this configuration the system is stable in the sense that it tries to minimize the deviation. Based on eq. (17) the force on the Target $\mathbf{F}_t$ is:

$$\mathbf{F}_t = m_t \cdot \begin{bmatrix} I_1^{-1} & 0 & 0 \\ 0 & I_2^{-1} & 0 \\ 0 & 0 & I_3^{-1} \end{bmatrix} \cdot \left(\begin{bmatrix} d_x \\ d_y \\ d_z \end{bmatrix} \times \begin{bmatrix} F_{thr} \\ 0 \\ 0 \end{bmatrix} \right) \times \begin{bmatrix} l_x \\ l_y \\ l_z \end{bmatrix} = \\ = m_t \cdot \begin{bmatrix} (l_z d_z \text{-} l_y d_y) I_1^{-1} \\ \text{-} d_y I_2^{-1} \\ \text{-} d_z I_3^{-1} \end{bmatrix} \cdot l_x F_{thr} \tag{19}$$

with $\mathbf{r}_{dev} = [d_x \ d_y \ d_z]^T$ and $\mathbf{r}_{st} = [l_x \ l_y \ l_z]^T$; $\mathbf{I}_{sys}$ is assumed to be diagonal. Since only the lateral force is of concern, the x-component of $\mathbf{F}_t$ isn't relevant.
Assuming that l_x and F_{thr} are positive, the lateral force is $\mathbf{F}_l = c \cdot [0 \ \text{-}d_y \ \text{-}d_z]^T$. Therefore it is always directed opposite to the deviation, showing the properties of a spring force. Because of this, the system engages in a stable oscillation, where the two bodies slide against each other. If damping is provided, by either a small force of friction or the robot, the system will converge on the state $\mathbf{r}_{dev} = 0$. This is very advantageous since it also eliminates the external torque resulting from the deviation. In this case the Chaser's attitude controller doesn't need to compensate for any disturbances and the system is balanced, allowing it to fly on a straight trajectory.
While the robot exerts forces in the y- or z-direction it also needs to provide a torque τ_x about the x-axis. The magnitude of this torque is dependent on the radius of the grasping point, represented by $\mathbf{r}_l$ in equation (16). The robot forces in the frictionless case aren't conditioned by the inertial forces in the system itself. The system oscillates stably and the robot must only provide damping in an amount that it can handle.

4. BOOST CONTROL

For the deorbiting boost the thrust vector of the orbit control system should pass through the CoM and the orientation of the composite system is established such that the boost decreases orbital velocity, i.e. the boost direction corresponds to antiflight direction. Fixed body mounted orbit control thrusters (OCT) have a fixed force vector. Due to the disturbance torques the firing of the thrusters may cause disturbance torques as discussed in Subsection 3.1. These disturbance torques may be larger than the torque capabilities of the attitude control system since the OCT provide thrust of a higher order of magnitude than the attitude control thrusters.
For high-thrust-level single OCS engines thus requires a gimballing of the engine. If a cluster of thrusters with modulation capability is applied, the disturbance torques can be counteracted by OFF modulation. This is the selected approach in this scenario. Here, four engines of $375\,\mathrm{N}$ each are used to perform the deorbiting burn (order of $50\frac{\mathrm{m}}{\mathrm{s}}$ per burn). For the given $9.4\,\mathrm{t}$ mass this gives burn durations of around $5\,\mathrm{min}$.
For the manipulator arm the acceleration disturbance due to the OFF modulation needs to be analyzed. Therefore the control principle during boost has been simulated for a small boost of $100\,\mathrm{s}$ duration, assuming a symmetric thruster accommodation of $0.5\,\mathrm{m}$ (y-z from the x-axis) with a CoM deviation of $8\,\mathrm{cm}$ in the y- and $10\,\mathrm{cm}$ in the z-direction). As can be seen in Fig. 7 the total force along the axial is not constant but varies due to OFF modulation. Since the overall thruster OFF time is known on board, the total boost duration must be extended accordingly to account for these phases. With a simple pulse width modulation up to three thrusters may be OFF commanded simultaneously for a short period. Accordingly the total acceleration drops to one forth of the max for a short period. To avoid vibrational motion of the client at the contact surface the drop at a time should be limited to one and the total drop should stick to half the total thrust level (see 2.2.3). This can be achieved with a more sophisticated modulation, e.g. OFF modulation for two thrusters is performed at the beginning of the control cy-

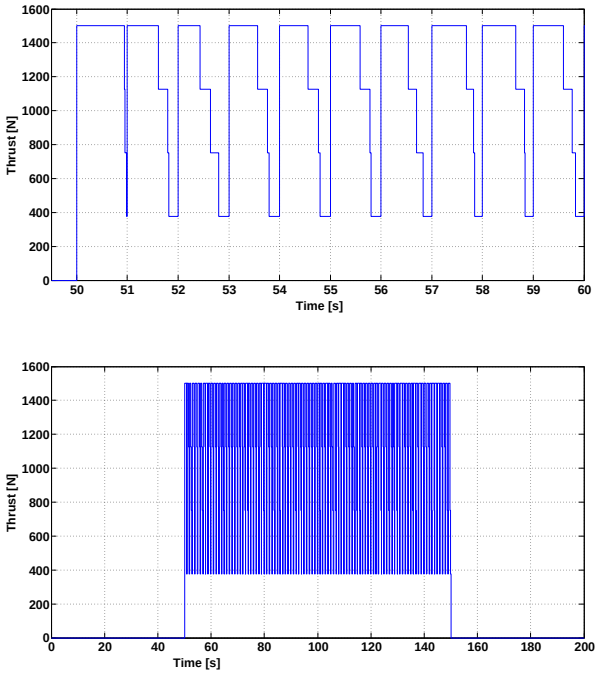

Figure 7: Off modulated Boost Thrust Profile. The upper figure shows a close up view of the individual steps, the lower shows the complete profile of the burn.

cle and for the others at the end of the cycle. Generally however this will impose a stronger limitation in the tolerance for CoM position and needs to be analysed in view of the thruster accommodation and the needs.
In conjunction with the results of Section 2.2.3 this shows that while the off-modulation has an influence on the stability of the system it can be configured in such a way, that the system remains in contact at all times and is therefore stable.

5. NUMERICAL SIMULATION

SIMPACK is a commercial tool for multi-body simulations. It features a graphic interface that allows the user to create bodies and specify their mechanical properties. The bodies can be connected with force elements such as springs, dampers or external forces, as well as mechanical joints. Subsequently, the equations of motion of the system can be numerically integrated over a period of time while the program records the positions, velocities and accelerations of each body as well as the forces in the force elements. This data is recorded into a file. With the help of the post-processor the values of a property can be displayed in a graph and compared to other properties.
Several cases were simulated using such a model, leading to results showing the motion of the satellites and the forces between them.

5.1. Simpack Model

The SIMPACK model shown in Figure 1 consists of two solid bodies. Their shape isn't relevant; the graphics were only included to make the system look more realistic. The system was built around a system coordinate frame located in the point where the two satellites contact. The positions of each body's CoM is given in this frame. The Chaser has the following properties:

- Mass = 1200 kg
- $\mathbf{I} = \begin{bmatrix} 650.0 & -10.0 & 22.0 \\ -10.0 & 950.0 & -4.0 \\ 22.0 & -4.0 & 950.0 \end{bmatrix}$ kg · m^2 *(body frame)*
- Location of the CoM = $\begin{bmatrix} -1.225 & 0 & 0 \end{bmatrix}^T$ m *(expressed in the system coordinate frame)*

The properties of the Target are:

- Mass = 8200 kg
- $\mathbf{I} = \begin{bmatrix} 10000 & 0 & 0 \\ 0 & 226000 & 0 \\ 0 & 0 & 228000 \end{bmatrix}$ kg · m^2 *(body frame)*
- Location of the CoM = $\begin{bmatrix} 5 & 0 & 0 \end{bmatrix}^T$ m *(without deviation of the CoM, expressed in the system coordinate frame)*
- Orientation = $\begin{bmatrix} 0 & 0 & \frac{\pi}{2} \end{bmatrix}^T$ *(roll pitch yaw)*

The combined system has these properties:

- Mass = 9400 kg
- $\mathbf{I} = \begin{bmatrix} 226650 & -10.0 & 22.0 \\ -10.0 & 515730 & -4.0 \\ 22.0 & -4.0 & 269570 \end{bmatrix}$ kg · m^2
- Location of the CoM = $\begin{bmatrix} 4.205 & 0 & 0 \end{bmatrix}^T$ m *(without deviation of the CoM, relative to global coordinate frame)*

The system's moments of inertia are dependent on the configuration in which the two satellites connect. In the configuration that was used, the Chaser connects to one of the long sides of the Target. Because of this the moment I_{yy} of the system inertia is significantly smaller than the moments I_{xx} and I_{zz}. Therefore a torque about the current y-axis results in a greater angular acceleration than one about the z-axis. The effects can be seen in the numeric simulations of Subsection 5.2. If the Chaser can connect to the smallest side, the two larger moments of inertia are located on the axes which correspond to the axes that torques deriving from deviations of the CoM would act about. Such a configuration would experience

lower angular accelerations and would therefore cause smaller lateral forces.

The surface contact is simulated by six spring-damper elements arranged in a hexagon with a radius of $0.8\,\mathrm{m}$. Each has a stiffness in the x-direction of $10000\,\frac{\mathrm{N}}{\mathrm{m}}$ and a damping of $3000\,\frac{\mathrm{Ns}}{\mathrm{m}}$. The stiffnesses in the y- and z-directions are zero, meaning that the force elements don't transfer any force in these directions. These force elements are only used to model the normal forces; friction is modelled by a separate force element. The coefficients of the springs and dampers must be very large in relation to the masses present in the system to minimize oscillations. Without oscillations, only the three-dimensional dynamics of the system are present.
The location where each of these forces acts is of interest, since the difference in force between opposing components creates a moment which ensures the balance of torques on the target mass (see eq. (16)). The deviation of the Target CoM used for the following simulations is $[0 \;\; 0.35 \;\; 0.35]^T$ m. These values were chosen in order to satisfy the condition that the vector between the CoM of Target and Chaser should point mainly in the x-direction. With the distance in the x-direction of $6.23\,\mathrm{m}$, that was used, the vector connecting the centers of mass has an angle of $5°$ to the x-axis. The values for the deviation were chosen purposely high to demonstrate the stability of the system in this analysis.
The thrust force used to propel the system is $1500\,\mathrm{N}$.
In the following simulations there is no attitude control. With external torque acting the satellites, the bodies start rotating, which will lead to a tumbling motion. This scenario is sufficient though to show the stability of the system and the magnitude of the robot forces and torques. The attitude controller that would be used on the Chaser can selectively turn off one or several thrusters. Doing this doesn't increase the lateral forces, which are linearly dependent on the thrust force.

5.2. Simulation Results

Using the model described in the previous Subsection simulations were conducted examining the case involving friction and the frictionless case (discussed in 3.3.1 and 3.3.2).

5.2.1. Simulation with Friction

The simulation of friction was conducted with the help of a force element that prevents lateral movement. Due to the external torque resulting from a deviation in the y- and z-direction the system experiences an angular acceleration in both these directions relative to the different moments of inertia. The simulation was only conducted for $50\,\mathrm{s}$ since the system performs several revolutions in that time. Figure 8 shows that initially there is an angular acceleration for the component gamma (which corresponds with the z-axis) and beta (which corresponds with the y-axis). The acceleration about the y-axis is greater since the same torque combined with a smaller moment of inertia about this axis results in a greater acceleration.

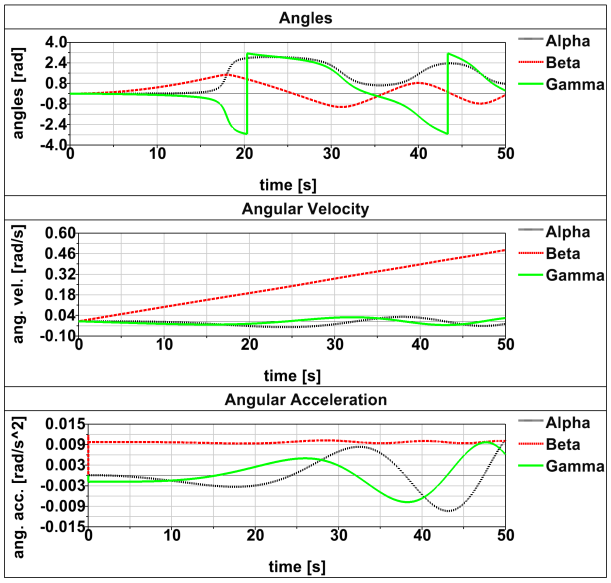

Figure 8: Angular components of the case with friction. The angular accelerations (which cause lateral forces) in the y- and z-direction are initially constant and oscillate subsequently due to the distribution of the moments of inertia.

After some time has passed the system starts tumbling and some components oscillate. In a system with attitude control the components would be limited to a lower level and tumbling would thus be prevented. The lateral forces in the lower half of Figure 9 initially level out at an absolute value of $65\,\mathrm{N}$. The six contact forces in the upper half of Figure 9 transmit the normal force. Its value is $\frac{m_t}{m_t+m_s} \cdot 1500\,\mathrm{N} = 1309\,\mathrm{N}$. The difference in the forces accounts for the torques about the y- and z-axis transmitted from the Chaser to the Target. The overall contact force decreases over time as the angular velocity increases. Subsection 3.1 states that ω_s causes an inertial force that opposes the thrust force. After $38\,\mathrm{s}$ one of the contact forces crosses into the positive range, soon fol-

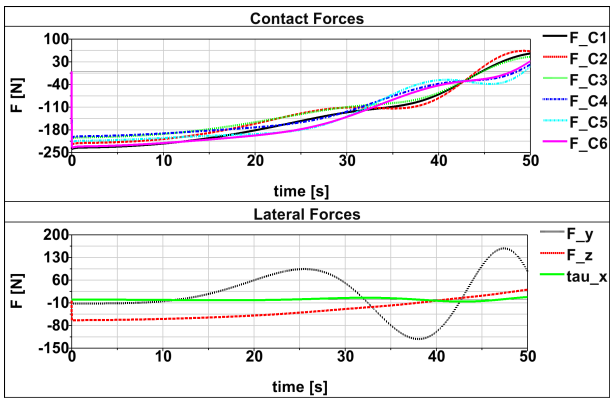

Figure 9: Forces of the case with friction. The difference in the six contact forces is related to the torque being transferred between the bodies. The second graph shows the overall lateral forces that are compensated by friction

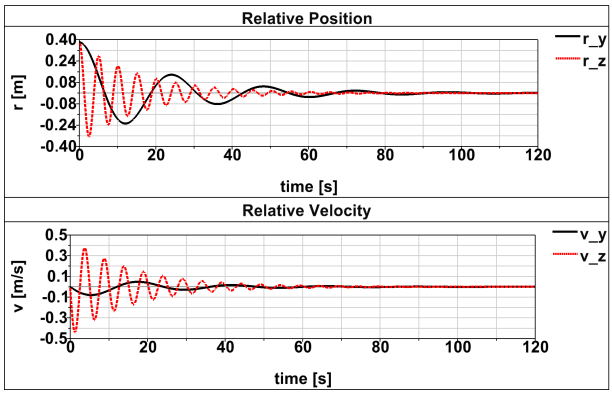

Figure 10: Relative position and velocity of the frictionless case. This shows the dampened oscillation between the two bodies starting from an initial deviation and converging on the point where no deviation is present.

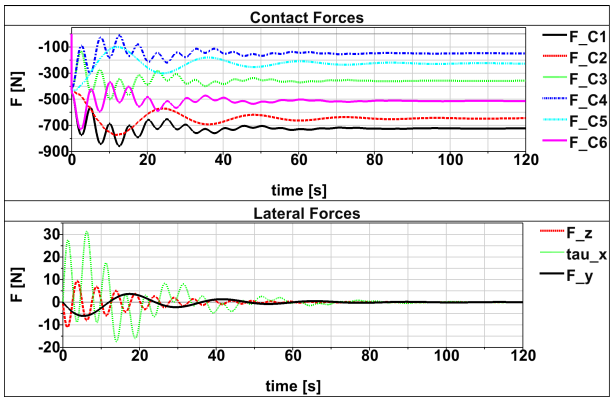

Figure 11: Forces of the frictionless case. Since the lateral forces only provide damping in this case, the forces are only dependent on the relative velocity of the two bodies.

lowed by the other contact forces, which would lead to separation of the two bodies. For this reason the attitude controller cannot tolerate an angular velocity greater than a certain value.
The torque about the x-axis τ_x lies within a range of $\pm 5\,\mathrm{Nm}$.

Considering a coefficient $\mu = 0.5$, friction could compensate the lateral forces and τ_x for roughly $40\,\mathrm{s}$ in this scenario. This easily covers all the angular accelerations and velocities that a controlled system would experience. Since the controller wouldn't allow great angular velocities to build up, the first few seconds of the simulation are especially relevant.

5.2.2. Simulation of the Frictionless Case

In this case the contact surface was assumed to be perfectly smooth, the lateral forces and the corresponding torque are provided solely by the robot. The robot follows a control law that only provides damping, no elasticity. Therefore the system will engage in a dampened oscillation as shown in Figure 10. The frequency of the oscillation in the z-direction is greater than the frequency of the y-direction since the angular velocities of the oscillation are dependent on the terms $d_y \cdot I_2^{-1} l_x F_{thr}$ and $d_z \cdot I_3^{-1} l_x F_{thr}$. Since I_2 is smaller than I_3 the resulting angular velocity is greater.
The deviation starts out at $0.38\,\mathrm{m}$ in both directions and goes to zero, eliminating the external torque.
The lateral forces F_y and F_z shown in Figure 11 follow the relative velocities of Figure 10. The damping factors used for this simulation are $75\frac{\mathrm{Ns}}{\mathrm{m}}$ in the y-direction and $25\frac{\mathrm{Ns}}{\mathrm{m}}$ in the z-direction. This is done to improve the convergence of the y-component while reducing the damping force needed for the movement in the z-direction. This leads to a maximum robot force of $6.0\,\mathrm{N}$ for F_y and $11.2\,\mathrm{N}$ for F_z. The torque τ_x depends on the robot grasping point; the vector used for this simulation is $\begin{bmatrix}0 & 2.5 & 2\end{bmatrix}^T\,\mathrm{m}$. This leads to a maximum torque of $31.0\,\mathrm{Nm}$.

The contact forces shown in the upper half of Figure 11 assume different values to ensure the balance of torques. All components remain in the negative range, which means that there is always compression.

The simulation of the frictionless case shows that the system is inherently stable and only needs damping to cause convergence. The results can also be applied to a case, in which there is a low amount of friction that permits the bodies to move relative to each other. Since the system approaches a state in which there is no external torque, a case with low friction is preferable to one with high friction, a fact that should be considered in the design of the Chaser's contact points.

6. CONCLUSION AND FURTHER WORK

The previous sections have shown that the proposed deorbiting mission is possible with the proposed method. The potential energy is low if the structure has high stiffness. The lateral forces resulting from external torque can be considerable, but they are either compensated by friction or absorbed in oscillation.
It is shown that a standard off-modulation boost control method is sufficient or may even be adapted to ensure that no separation takes place between the satellites during the deorbiting maneuver.
Some aspects such as the geometry of the chaser, the friction in the contact points or the stiffness of the satellite structure are important and need to be considered in the design of the chaser.